
This is an electronic reprint of the original article.
This reprint may differ from the original in pagination and typographic detail.

Liu, Peng; Khan, Abu Taher; Ding, Er Xiong; Zhang, Qiang; Xu, Zhenyu; Bai, Xueyin; Wei, Nan; Tian, Ying; Li, Diao; Jiang, Hua; Lipsanen, Harri; Sun, Zhipei; Kauppinen, Esko I.

Direct Synthesis of Semiconducting Single-Walled Carbon Nanotubes Toward High-Performance Electronics

Published in:
Advanced Electronic Materials

DOI:
[10.1002/aelm.202300196](https://doi.org/10.1002/aelm.202300196)

Published: 01/07/2023

Document Version
Publisher's PDF, also known as Version of record

Published under the following license:
CC BY

Please cite the original version:
Liu, P., Khan, A. T., Ding, E. X., Zhang, Q., Xu, Z., Bai, X., Wei, N., Tian, Y., Li, D., Jiang, H., Lipsanen, H., Sun, Z., & Kauppinen, E. I. (2023). Direct Synthesis of Semiconducting Single-Walled Carbon Nanotubes Toward High-Performance Electronics. *Advanced Electronic Materials*, 9(7), Article 2300196.
<https://doi.org/10.1002/aelm.202300196>

This material is protected by copyright and other intellectual property rights, and duplication or sale of all or part of any of the repository collections is not permitted, except that material may be duplicated by you for your research use or educational purposes in electronic or print form. You must obtain permission for any other use. Electronic or print copies may not be offered, whether for sale or otherwise to anyone who is not an authorised user.

Direct Synthesis of Semiconducting Single-Walled Carbon Nanotubes Toward High-Performance Electronics

Peng Liu, Abu Taher Khan, Er-Xiong Ding, Qiang Zhang,* Zhenyu Xu, Xueyin Bai, Nan Wei, Ying Tian, Diao Li, Hua Jiang, Harri Lipsanen, Zhipei Sun, and Esko I. Kauppinen*

The large-scale synthesis of high-purity semiconducting single-walled carbon nanotubes (s-SWCNTs) plays a crucial role in fabricating high-performance and multiapplication-scenario electronics. This work develops a straightforward, continuous, and scalable method to synthesize high-purity and individual s-SWCNTs with small-diameters distribution (≈ 1 nm). It is believed that the water and carbon dioxide resulting from the decomposition of isopropanol act as oxidizing agents and selectively etch metallic SWCNTs, hence enhancing the production of s-SWCNTs. The performance of individual-SWCNTs field effect transistors confirms the high abundance of s-SWCNTs, presenting a mean mobility of $376 \text{ cm}^2 \text{ V}^{-1} \text{ s}^{-1}$ and a high mobility of $2725 \text{ cm}^2 \text{ V}^{-1} \text{ s}^{-1}$ with an on-current to off-current ($I_{\text{on}}/I_{\text{off}}$) ratio as high as 2.51×10^7 . Moreover, thin-film transistors based on the as-synthesized SWCNTs exhibit excellent performance with a mean mobility of $9.3 \text{ cm}^2 \text{ V}^{-1} \text{ s}^{-1}$ and $I_{\text{on}}/I_{\text{off}}$ ratio of 1.3×10^5 , respectively, verifying the enrichment of s-SWCNTs. This work presents a simple and feasible route for the sustainable synthesis of high-quality s-SWCNTs for electronic devices.

1. Introduction

High-performance microprocessors based on field-effect transistors (FETs) are the foundation of electronic devices that pervade every aspect of life and accelerate the progress of modern industry as well as our daily lives. However, due to the role of quantum effects in small-scale FETs, the size of traditional silicon-based FETs can hardly be reduced indefinitely, and the well-known Moore's Law is reaching its limit. Therefore, the traditional silicon-based FETs will be out of its depth in future revolutionary technologies.^[1–4] To meet the increasing demands of high performance and more complex application scenarios of electronic devices, researchers have been exploring new electronic materials to

P. Liu, A. T. Khan, Q. Zhang, Z. Xu, H. Jiang, E. I. Kauppinen
Department of Applied Physics
Aalto University School of Science
Puumiehenkuja 2, Aalto, Espoo 00076, Finland
E-mail: qiang.zhang@aalto.fi; esko.kauppinen@aalto.fi
P. Liu, E.-X. Ding, X. Bai, D. Li, H. Lipsanen, Z. Sun
Department of Electronics and Nanoengineering
Aalto University
Espoo FI-00076, Finland
Q. Zhang
Honda Research Institute USA
Inc. 70 Rio Robles, San Jose, CA 95134, USA

N. Wei
Research Center for Carbon-based Electronics
Peking University
Beijing 100871, China
Y. Tian
School of Science
Dalian Maritime University
Dalian 116026, China
Z. Sun
QTF Centre of Excellence
Department of Applied Physics
Aalto University
Espoo FI-00076, Finland

 The ORCID identification number(s) for the author(s) of this article can be found under <https://doi.org/10.1002/aelm.202300196>

© 2023 The Authors. Advanced Electronic Materials published by Wiley-VCH GmbH. This is an open access article under the terms of the Creative Commons Attribution License, which permits use, distribution and reproduction in any medium, provided the original work is properly cited.

DOI: 10.1002/aelm.202300196

replace silicon. Single-walled carbon nanotubes (SWCNTs) have been proven to be an ideal alternative channel material for FETs owing to their unique structure, excellent electrical properties, and stability.^[2,5,6] For example, the small tube diameter and quasi-1D topology of SWCNTs, can largely minimize short-channel effects, thus enable the excellent gate control at an extreme device scaling (gate length lower than 10 nm).^[5–7] In addition, the superior chemical and mechanical stability of SWCNTs combined with their outstanding flexibility, open the opportunity for devices to function under extreme operating conditions (high/low temperature, strain, etc.).^[6] Since Tans et al. reported the first p-type SWCNT transistor in 1997,^[8] SWCNT-FETs technology has intensively been developed over the last 20 years. For instance, Hills et al. corroborated the feasibility of integrating SWCNT-FETs, and the microprocessor containing more than 14 000 complementary metal-oxide-semiconductor FETs.^[9] Furthermore, Liu et al. reported that CNT-based FETs outperform that of commercial silicon metal oxide-semiconductor FETs with similar gate lengths in several key performance metrics.^[2] Despite of the remarkable advances, the large-scale fabrication and industrialization of SWCNT-FETs are still facing challenges.^[10,11] Since CNTs can be either metallic or semiconducting, naturally forming about one-third of metallic CNTs during the uncontrolled synthesis process,^[6,12] the large-scale production of high-purity s-SWCNTs with outstanding electrical quality is a key factor for electronics application.

Great efforts have been devoted to developing a controlled preparation process for high-purity s-SWCNTs. There are mainly two pathways to achieve this goal so far:^[6,13] 1) post-synthesis sorting,^[14–17] and 2) direct synthesis.^[18–20] The sorting methods mainly include density gradient ultracentrifugation,^[14] column chromatography,^[15] ion exchange chromatography,^[16] and conjugated polymer extraction.^[17] However, the unavoidable intensive sonication and introduction of dispersants in those methods could lead to uncontrolled contamination of SWCNTs and destruction of the structure, thus impairing their intrinsic properties.^[12,21,22] In regard to direct synthesis, the important strategy is to introduce an oxidizing environment (methanol,^[19,23] water vapor^[20,24,25] and oxygen,^[26] etc.) during the synthesis process, to inhibit the growth of metallic-SWCNTs (m-SWCNTs) or to etch them. Liu et al.^[19] utilized a mixture of ethanol/methanol as a carbon source, proposing that methanol (as a weak etchant) preferentially etch most of the m-SWCNTs on substrates, resulting in enriched s-SWCNTs on substrates. In addition, Zhou et al.^[20] found that a suitable water concentration plays a key role in the selective growth of s-SWCNTs. They achieved dominant growth of s-SWCNTs using isopropanol (IPA) as a carbon source via a substrate CVD method and found it to be superior to ethanol. This was attributed to the fact that IPA could provide a higher water concentration than ethanol. Despite the reported high-purity s-SWCNTs, they were mostly obtained on the substrate growth process with low yield.^[22] Ding et al.^[23] made their efforts on the floating catalyst chemical vapor deposition (FCCVD) system to synthesize enriched s-SWCNTs based on mixed carbon sources (methanol and ethanol), while they obtained a low yield of high-purity s-SWCNTs with poor reproducibility. Batch synthesis of high-purity s-SWCNTs with reasonable selectivity and good reproducibility has still been a far goal to reach by far. In addition, it will be interesting to study

and certify the superiority of IPA in the selective synthesis of s-SWCNTs in FCCVD systems. A thoughtful understanding of the effect of thermodynamic and kinetic factors on the chirality distribution is also demanded, especially on the direct controllable synthesis of high-purity s-SWCNTs by FCCVD.

In this study, we adopted a laboratory-designed FCCVD system and used IPA as the carbon source for controlled synthesis of s-SWCNTs. The scheme of the experimental setup is shown in Figure S1, Supporting Information. Rather than a mixture of carbon sources,^[19,23] the utilization of IPA is free from the effect of multiple carbon precursors, thus is advantageous for the mechanism investigation. Besides, the IPA-ferrocene method is safer and less toxic than other methods utilizing certain hydrocarbons, or carbon monoxide. In addition, we have systematically investigated the effects of temperature, feed rate, and H₂ flow rate on the purity of s-SWCNTs. We demonstrated a sustainable synthesis of s-SWCNTs films with 90% transmittance (T), high purity up to 94%, and a yield of 0.28 cm² h⁻¹. Additionally, both the electron diffraction analysis and individual-SWCNTs FETs statistics verified the high purity of s-SWCNTs. The highest mobility of our s-SWCNTs FETs reached 2725 cm² V⁻¹ s⁻¹ with a high on-current to off-current ($I_{\text{on}}/I_{\text{off}}$) ratio of 2.51 × 10⁷. Furthermore, the thin-film transistors (TFTs) simultaneously demonstrated a mean mobility of 9.3 cm² V⁻¹ s⁻¹ and a mean $I_{\text{on}}/I_{\text{off}}$ ratio of 1.3 × 10⁵. This demonstrates the great application potential of our large-scale synthesized SWCNTs in the field of electronics.

2. Results and Discussion

All optical absorption spectra (Figure 1a,c,e) show distinct characteristic peaks of the first and second inter-band transitions of s-SWCNTs (S_{11} and S_{22}), and the first inter-band transition of their metallic counterparts (M_{11}), proving the successful synthesis of SWCNTs. In addition, the low I_D/I_G ratio (≈ 0.05) in the Raman spectra (Figure S2a, Supporting Information) indicates the high-quality of as-synthesized SWCNTs.^[20] The highest synthesis temperature resulted in low and broad S_{11} peaks (980 °C in Figure 1a), suggesting a relatively broad diameter distribution and larger diameter of as-synthesized SWCNTs (Figure S3a, Supporting Information). This result is in a good agreement with the previous reports,^[27,28] showing that high temperature usually leads to large diameters and broad chirality distribution of SWCNTs. In contrast, SWCNTs synthesized at a lower temperature produced higher and narrowed S_{11} peaks, accompanied by blue-shifted peaks, and the mean diameter decreased to 0.94 nm from 1.08 nm. Moreover, the diameter distributions of SWCNTs demonstrated that $\approx 72\%$ of the product collected at 880 °C were in the range of 0.75–1.15 nm. Interestingly, a high purity of $\approx 93\%$ was obtained for the as-synthesized s-SWCNTs at 880 °C (Figure 1b). It is worthy to mention that the obtained results were repeatable, indicating the excellent reactor stability and reproducibility of the s-SWCNTs (Figure S2b, Supporting Information). The good reproducibility is attributed to applying of IPA (instead of the mixed carbon source) and strict experimental control (dedicated quartz tube and reactor). Besides, the purity of s-SWCNTs followed a trendline, which initially increased and then decreased with an increase in temperature. This could be attributed to the rapid decomposition of feedstocks and the nucleation of catalysts at high temperatures, resulting in the

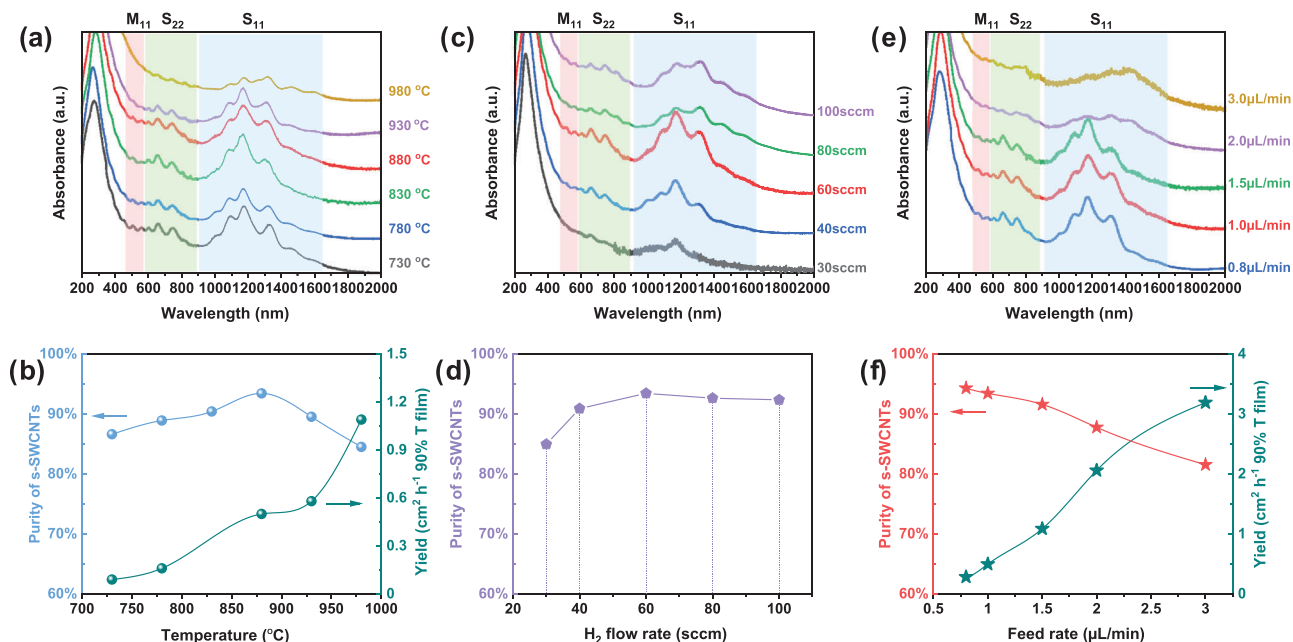


Figure 1. Optical characterizations of SWCNTs samples under different synthesis parameters. a) Absorption spectra of s-SWCNTs collected at different temperature. The three-color region from left to right represents the M₁₁, S₂₂, and S₁₁ regions, respectively. b) Purity and yield (cm² h⁻¹ 90% T film) of s-SWCNTs at different temperatures. The feed rate and H₂ flow rate are 1.0 µL min⁻¹ and 60 standard cubic centimeters (sccm), respectively (synthesis parameters of (a) and (b) are 1.0 µL min⁻¹ and 60 sccm H₂, following the same). c) Absorption spectra of SWCNTs collected at different H₂ flow rates. d) Purity of s-SWCNTs. Synthesis parameters of (c) and (d) are 880 °C – 1.0 µL min⁻¹. e) Absorption spectra of SWCNTs collected at different feedstock feed rates. f) Purity and yield (cm² h⁻¹ 90% T film) of s-SWCNTs at varied feed rates. Synthesis parameters of (e) and (f) are 880 °C – 60 sccm H₂.

uncontrolled growth of SWCNTs, and increased production yield of SWCNTs (Figure 1b). This indicates that the high-temperature environment was not conducive to the controlled growth of s-SWCNTs.^[29] Raman characterization further supported our findings on the effect of temperature on the purity of s-SWCNTs. As shown in Figures S4b,c, Supporting Information, the same resonant SWCNTs of the samples were excited by 514 nm and 633 nm lasers, respectively. While the radial breathing mode (RBM) intensities of m-SWCNTs were enhanced with the temperature, indicating that more m-SWCNTs were synthesized. However, the synthesis of s-SWCNTs could not be achieved at low temperature either. As shown in Figure 1b, both the yield and purity of s-SWCNTs were low when the synthesis temperature was lower than 850 °C. The reason for low yield is believed to be the insufficient decomposition of the feedstock at lower temperatures. For the low purity, we hypothesized that the low temperature was not preferred for the selective formation of catalyst seeds that were beneficial for the s-SWCNTs synthesis. In addition, the activity of the etchant (CO₂) is affected by temperature,^[30] and the selective etching efficiency of m-SWCNTs decreases at low temperature. Obviously, the as-synthesized SWCNTs at a lower temperature, had a signal peak of a new chirality of m-SWCNT excited by the 514 nm laser (Figure S4b, Supporting Information).

The effect of H₂ flow rate on purity of s-SWCNTs was also investigated under the optimum synthesis temperature of 880 °C. The absorption spectra of the synthesized SWCNTs in different H₂ flow rates (30–100 sccm) are presented in Figure 1c. The highest peak position of S₁₁ remained as the H₂ flow rate gradually increased from 30 sccm to 60 sccm. However, with the additional increase of the H₂ flow rate, a redshift of the high-

est S₁₁ peak was observed, indicating that the mean diameter of the s-SWCNTs was increased.^[23] The diameter distribution diagram (Figure S3b, Supporting Information) clearly showed that the mean diameter of SWCNTs increased by ≈0.1 nm with the increase of H₂ flow rate from 30 sccm to 100 sccm. This trend also agrees with our previous report^[23] that the mean diameter of SWCNTs can be adjusted by the H₂ flow rate. It is worth noting that at the low H₂ flow rate (30 sccm) ≈63% of the SWCNTs possessed a sub-nanometer diameter, while this proportion decreased to 46% when the H₂ flow rate is increased to 100 sccm. The above-mentioned phenomenon indicated a preferential etch effect of H₂ on small-diameter SWCNTs.^[31] The more important fact was that the purity of s-SWCNTs raised with H₂ flow rate until 60 sccm (Figure 1d). This enrichment of s-SWCNTs by H₂ could be attributed to the high reactivity between H₂ and m-SWCNTs (relatively smaller ionization potential) compared to s-SWCNTs with the similar diameters.^[19,32] This phenomenon was supplementary supported by the Raman spectra (Figure S5, Supporting Information), where the RBM signal intensity excited by four different wavelength lasers was decreased in the small diameter SWCNTs region, under high H₂ flow rate.

To systematically investigate the synthesis parameters affecting the purity of s-SWCNTs, the feedstock rate was also varied. Optical characterizations of the obtained SWCNTs at different feedstock rates are shown in Figure 1e. In our premixed feedstock design, the amount of carbon source and catalyst increased linearly with feed rates. A high feed rate led to a large amount of catalyst aggregation, resulting in s-SWCNTs with larger mean diameters (higher resistance to etchant) (Figure S3c, Supporting Information) and lower purity (Figure 1f). Meanwhile, the

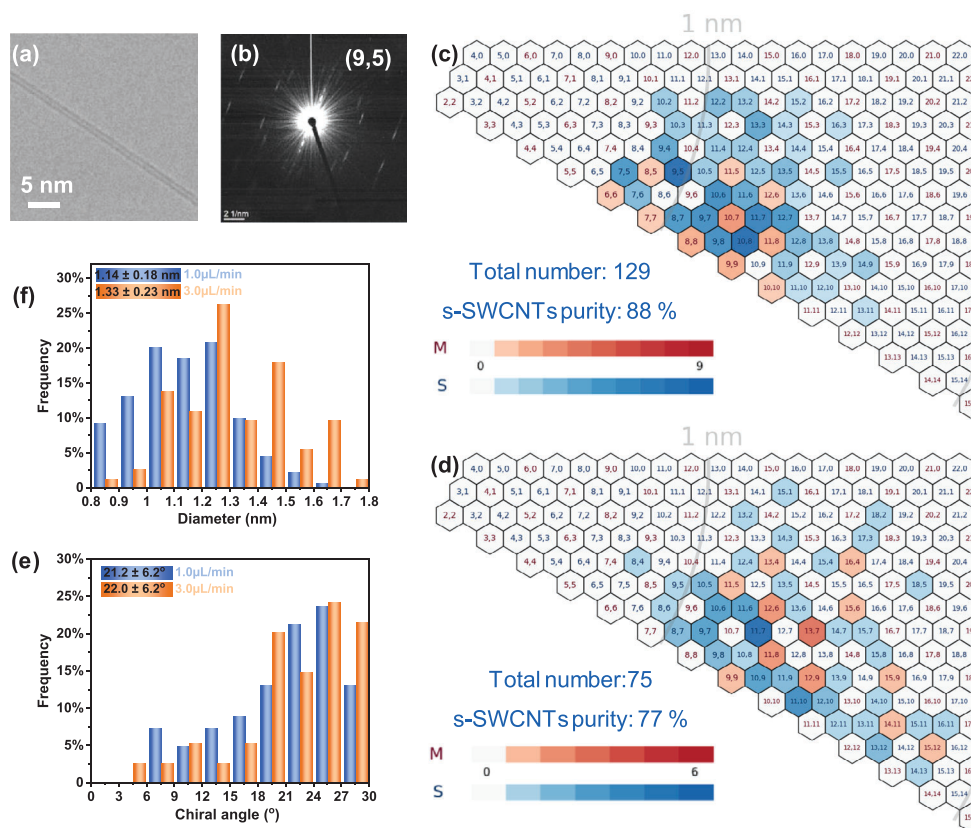


Figure 2. Determination of chirality and the purity of s-SWCNTs by electron diffraction technique. a) A representative TEM micrograph of an individual SWCNT; b) the corresponding electron diffraction pattern and the determined chirality index. c) Chirality map of as-synthesized SWCNT samples at 880 °C–1.0 $\mu\text{L min}^{-1}$ –60 sccm H_2 . M and S represent m-SWCNTs and s-SWCNTs, respectively. d) Chirality map of as-synthesized SWCNT samples at 880 °C–3.0 $\mu\text{L min}^{-1}$ –60 sccm H_2 . e) Chiral angle distributions and f) Diameter distributions of SWCNTs presented in (c) and (d).

formation of amorphous carbon in larger amount could reduce the quality of SWCNTs, which could be observed from the high background contribution and the obvious decrease in the S_{11} peak intensity at high feed rate.^[33] The purity of s-SWCNTs was improved significantly with the decrease of feed rate (Figure 1e and Figure S6, Supporting Information). The purity of s-SWCNTs reached 88% accompanied by a yield $\approx 2.06 \text{ cm}^2 \text{ h}^{-1}$ 90%T film at feed rate of 2 $\mu\text{L min}^{-1}$ (Figure 1e). To improve the purity of s-SWCNTs, we decreased the feeding rate to a more extent. The purity reached the highest value (94%) with the feed rate reduced to 0.8 $\mu\text{L min}^{-1}$. In this case, structure-controllable synthesis of s-SWCNTs was achieved by sacrificing the yield.^[23]

Electron diffraction patterns of a large number of individual SWCNTs were acquired to map their chirality distribution (Figure S7, Supporting Information). A typical electron morphology and a diffraction pattern of an as-synthesized individual SWCNT are shown in Figure 2a and Figure 2b. At a feed rate of 1.0 $\mu\text{L min}^{-1}$, the chirality distribution of SWCNTs (Figure 2c) demonstrated higher purity of s-SWCNTs, and more concentrated chiral indices than those obtained at 3.0 $\mu\text{L min}^{-1}$ (Figure 2d), although their mean chiral angles were similarly centered on the near armchair region (Figure 2e). The purity of the synthesized s-SWCNTs determined by the electron diffraction patterns was 88%, which was $\approx 5\%$ lower than the purity ($\approx 93\%$) calculated from the absorption spectrum (Figure 1a). This discrepancy

could be attributed to the distinction between the absorption intensity based on bulky SWCNTs film, and the finite count based on microscopic individual SWCNTs. It was also implied that s-SWCNTs were longer than m-SWCNTs in our samples.^[23,34] Similarly, the diameter distribution of SWCNTs detected by the electron diffraction patterns (Figure 2f) was also slightly different from that of the absorption spectra (Figure S3c, Supporting Information), however, this could be neglected due to the samples' scale variation. It is important that the variation trend of the SWCNTs diameter with the feed rate was the same using the two detection methods.

To obtain information on the variation of s-SWCNTs purity, we performed an in-situ monitoring of gaseous reaction composition during the synthesis of SWCNTs using gas-phase FT-IR spectroscopy. The IR spectra of the gas composition obtained after filtration are shown in Figure 3a, and the results were analyzed using reference spectra of individual substances.^[35] Based on the IR spectra, the observed vibrational rotation bands can be assigned to CH_4 , H_2O , CO , CO_2 , etc. The dependence on the concentration of aerosol components at a total pressure $P_{\text{total}} = 750 \text{ mbar}$ on the set feed rates is shown in Figure 3b and Figure S8a. The concentration of CO and CH_4 (light purple area) obviously exceeded the contribution of the rest of the gas phase species, especially the proportions of acetylene (C_2H_2), ethylene (C_2H_4), ethane (C_2H_6) and toluene (C_7H_8) were all lower than

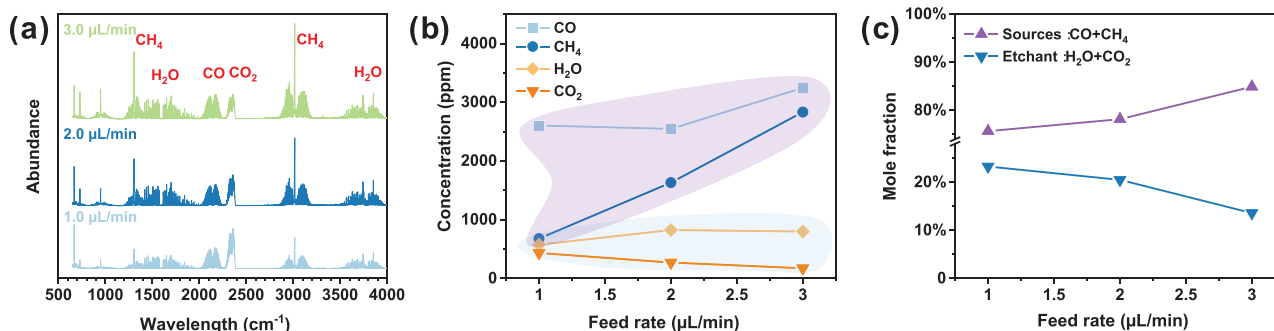


Figure 3. Investigation of the origin of s-SWCNT enrichment using a gas-phase FT-IR spectrometer (at 880 °C–60 sccm H₂). a) FT-IR spectra of the outlet reactor gas at varied feed rates. b) Feed rate versus the concentration of main decomposed products in the reactor outlet. c) Feed rate versus the mole fraction of main decomposed products in the reactor outlet.

0.5%. In addition, the concentrations of CO and CH₄ maintained high levels at each feed rate, indicating CO and CH₄ were the main gaseous products of IPA decomposition, and direct carbon sources for SWCNTs growth. This result was similar to the ethanol decomposition reported before.^[35] They claimed that the ethanol-ferrocene aerosol CVD combined the advantages of the two synthesis schemes (CO and CH₄), which enabled the production of pure SWCNTs with small diameters (≈1 nm). Besides, the CO-rich atmosphere favors the growth of high chiral angle SWCNTs requiring low activation energy for cap formation.^[29,36] Notably, the total mole fraction of H₂O and CO₂ increased significantly with the decrease of the feed rate (Figure 3c). It was proposed that H₂O could affect the nucleation of s-SWCNTs,^[20] and etch the unstable m-SWCNTs.^[23] Besides, CO₂ was reported to have a similar etching effect on m-SWCNTs.^[30] Therefore, the enrichment of s-SWCNTs in this work was achieved due to the synergistic effect of H₂O and CO₂ on etching. In addition, we performed multiple detections of the gas products under optimal conditions (Figure S8b, Supporting Information) and found only a small fluctuation in the concentration of the main gas components, indicating the good reproducibility of high-purity s-SWCNTs.

To evaluate the electrical properties of s-SWCNTs, the bundle length of the synthesized SWCNTs was measured before the TFT fabrication (Figure S9a, Supporting Information). The mean bundle length of SWCNTs collected under the optimized conditions was ≈6.38 μm (Figure S9b, Supporting Information), which was several times than that of typical solution-sorted SWCNTs (0.5–2.0 μm).^[17] The diameter and composition of the bundles were also analyzed (Figure S9c, Supporting Information), and found that ≈45% of the bundles were individual SWCNTs (diameters <1.5 nm were considered as an individual based on Figure 2f), while the rest were small bundles composed of 2 or 3 SWCNTs, with a mean bundle diameter of ≈2.37 nm. The purity of s-SWCNTs was additionally evaluated by electrical characterization of individual-SWCNTs FETs. **Figure 4a** illustrates a representative SEM image of the individual-SWCNTs FETs with a narrow channel length of 2 μm. Figure 4b exhibits the transfer curves ($I_d - V_{gs}$) measured at drain-source bias voltage $V_{ds} = -1$ V and gate-source sweeping voltage V_{gs} from -10 V to $+10$ V. A device was considered as working if drain to source current (I_d) is larger than 10 pA, and the working device was considered semiconducting if I_{on}/I_{off} ratio is >100, otherwise consid-

ered as metallic. Herein, 99 of 107 working devices were semiconducting FETs and the rest (8) were metallic FETs. Therefore, the ratio of semiconducting FETs was ≈92.5%, which is very similar to the s-SWCNTs purity detected by optical characterization (Figure 1b). This result additionally confirmed that our synthesis strategy could consistently produce highly enriched s-SWCNTs with good quality. In addition, SEM was used to check the number of bundles bridged by the electrodes. It was found that ≈50% of semiconducting FETs were bridged by individual-SWCNTs. The I_{on}/I_{off} ratio and charge carrier mobility (μ) are widely used metrics for describing the potential of SWCNTs for electronic applications.^[37] Here, the transfer curves showed p-type characteristics with excellent control over off-state current and a large variation in on-state current. Individual-SWCNTs FETs exhibited a mean I_{on}/I_{off} ratio of 8.33×10^6 with a maximum value of 5.24×10^7 , demonstrating the excellent switching control of SWCNTs-FETs (Figure 4c). Charge carrier mobility of 49 individual-SWCNTs FETs has been extracted from the linear region of transfer curves using the standard peak transconductance (PTC) method (shown in Supplementary text 2).^[23,38–40] The extracted mean PTC-mobility (μ_{PTC}) of individual-SWCNT FETs was $156.3 \text{ cm}^2 \text{ V}^{-1} \text{ s}^{-1}$, and the maximum value $663.3 \text{ cm}^2 \text{ V}^{-1} \text{ s}^{-1}$ with high I_{on}/I_{off} ratio of 5.16×10^7 (Figure 4c). Even though the PTC method proved the concrete evidence of good charge carrier mobility, the metal to SWCNT contact resistance has an adverse effect on the obtained mobility, in that the μ_{PTC} would be lower than the actual mobility of the channel. To avoid this effect, a more accurate estimation of charge carrier mobility was by the Y-function method (shown in Supplementary text 2).^[39] The extracted mean Y-function mobility (μ_{YF}) was $376 \text{ cm}^2 \text{ V}^{-1} \text{ s}^{-1}$ with a maximum value of $2725 \text{ cm}^2 \text{ V}^{-1} \text{ s}^{-1}$ (I_{on}/I_{off} ratio of 2.51×10^7), which is close to the theoretical limit for the 1 nm SWCNTs on SiO₂ substrates at room temperature (according to the theoretical analysis by Zhou et al.).^[41,42] This demonstrates the great application potential of our as-synthesized SWCNTs in the field of electronics.

Figure 4d shows the surface morphology of TFT channel area, filled by the as-synthesized SWCNTs film. In addition, the line density of our SWCNT film was as high as $3.9 \text{ CNTs } \mu\text{m}^{-1}$, which is much higher than those of the previously reported TFTs by detecting the gray value peak of SEM scanlines (Figure S10a).^[43,44] To accurately evaluate the intrinsic mobility of as-synthesized SWCNTs film, the $I_d - V_{ds}$ curve was plotted (Figure S10b). It

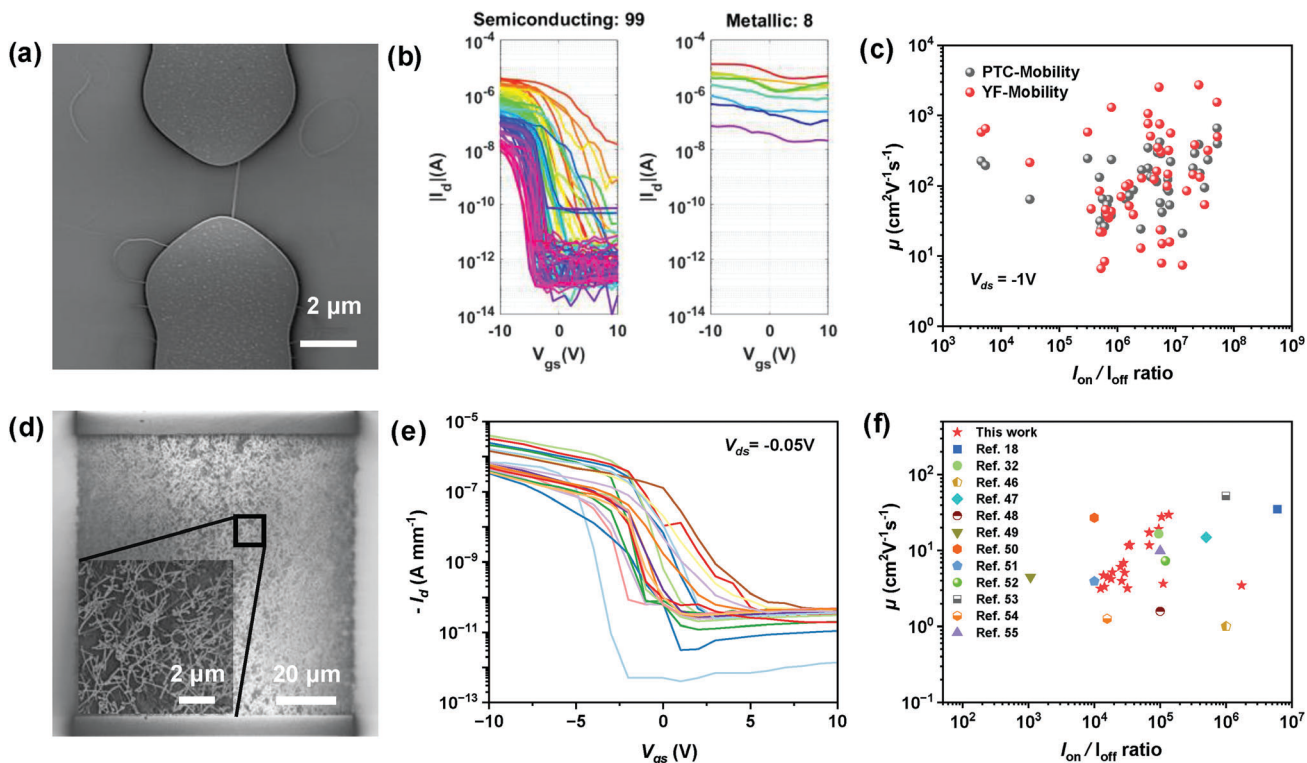


Figure 4. Electrical characterizations of SWCNT transistors. a) SEM image of a representative individual-SWCNTs FETs with a 2 μm channel length. b) Transfer characteristics of 115 SWCNT-FETs. c) μ_{FE} versus I_{on}/I_{off} ratio plots of the 49 individual-SWCNTs devices. d) SEM image of representative back-gated TFTs with channel length and width of 100 μm and SWCNTs film (the inset). e) Transfer characteristics of the TFTs. f) Comparison of our SWCNTs TFTs and other representative TFTs based on CNTs film. The SWCNTs samples were collected by the TP method at 880 $^{\circ}\text{C}$ –1.0 $\mu\text{L min}^{-1}$ –60 sccm H_2 .

was found that the $I_d - V_{ds}$ has a linear characteristic at various V_{gs} , which indicates that the contact of SWCNTs film with metal electrodes is an ohmic contact. Figure 4e presents the transfer curves of our fabricated TFTs at drain-source bias voltage $V_{ds} = -0.05$ V and gate-source sweeping voltage V_{gs} from -10 V to +10 V. Here, the common parallel plate model was used to extract the mobility (shown in Supplementary text 3),^[18,38,45] although this method would overestimate the capacitance of the SWCNTs film and thus underestimate the value of the extracted carrier mobility. Figure 4f and Supplementary table 1 show the mobility and the I_{on}/I_{off} ratio of 20 SWCNTs TFTs ($L_{ch} = 100 \mu\text{m}$), together with those of other TFTs based on CNTs film.^[18,32,46–55] The mean mobility and I_{on}/I_{off} ratio of our fabricated TFTs are $\sim 9.3 \text{ cm}^2 \text{ V}^{-1} \text{ s}^{-1}$ and $\sim 1.3 \times 10^5$, and the corresponding maximum values are $29.5 \text{ cm}^2 \text{ V}^{-1} \text{ s}^{-1}$ (with an I_{on}/I_{off} ratio of 1.35×10^5) and 1.72×10^6 (with a mobility of $3.5 \text{ cm}^2 \text{ V}^{-1} \text{ s}^{-1}$), respectively. Here, the moderate mobility is attributed to the relatively small diameter (~ 1 nm) of our synthesized SWCNTs, which have larger band gaps.^[41] Comparisons of the present TFTs with those representative TFTs reports, including TFTs based on the solution sorting s-SWCNTs with larger diameter,^[46,48–52,54] reveal that our fabricated TFTs have an advantage in flexible transistors and sensors^[45] as the latter requires tedious and harsh sorting process with low yield. The work is in progress to further improve the device performance through the selective synthesis of large-diameter s-SWCNTs, and the optimization of device parameters.

3. Conclusion

In this work, we report a continuous synthesis strategy for the production of highly individual semiconducting-SWCNTs with purity as high as 94%. The produced s-SWCNTs have a mean diameter ≈ 1 nm and a mean length $\approx 6.38 \mu\text{m}$. Under the optimized condition, the decomposition of IPA not only provided a carbon source for growing high-quality SWCNTs but also a suitable environment where s-SWCNTs are favored. In addition, as-synthesized s-SWCNTs exhibited excellent electrical properties with the mean mobility of $376 \text{ cm}^2 \text{ V}^{-1} \text{ s}^{-1}$ and I_{on}/I_{off} ratio up to 8.33×10^6 in individual-SWCNTs FETs. The high-performance TFT fabricated from the FCCVD high-purity s-SWCNTs exhibits high potential for their application in flexible electronics. To further enhance the TFT performance, employing additional sorting methods in the gas-phase environment to obtain a higher purity of s-SWCNTs with larger diameters could be affective methods. Besides, by further optimizing TFT parameters, it is foreseeable to enhance devices with better performance. Our synthetic strategy opens an important and feasible routine for continuous and large-scale production of s-SWCNTs that meets the needs of future electronic devices.

4. Experimental Section

Synthesis of s-SWCNTs: IPA ($\geq 99.5\%$, Sigma-Aldrich), ferrocene (98%, Sigma-Aldrich), and thiophene ($\geq 99\%$, Sigma-Aldrich) were uti-

lized as carbon source, catalyst, and promoter precursors, respectively. The preparation process of IPA feedstock is shown in Figure S1a. Ferrocene (0.25 wt.%) and thiophene (0.014 wt.%) were dissolved in IPA to form a liquid feedstock, which was injected into the system by a syringe pump (NE-1000 series, New Era Pump Systems, USA) at a feed rate of 0.6–3.0 $\mu\text{L min}^{-1}$. The feedstock was evaporated in a heated line maintained at 130 °C and carried by 300 sccm N_2 (vaporized from liquid nitrogen supplied by AGA, Finland, and then purified by an oxygen/moisture trap, OT3-4, Agilent) and 30–100 sccm H_2 (99.999%, Woikoski Oy, Finland) into the FCCVD reactor. The synthesis temperature was regulated in the range of 730 to 980 °C. As-synthesized SWCNTs film was collected at the outlet of the reactor using a MF-Millipore membrane filters ($\Phi = 25$ mm and thickness of 150 μm , Merck Millipore) with a pore size of 0.45 μm .

Characterizations of s-SWCNTs: After the s-SWCNTs film was transferred onto a quartz slide (35 mm \times 20 mm \times 1 mm, HSQ300, Finnish Special Glass Oy, Finland) by the press-transferred method (Figure S1c),^[56] an ultraviolet-visible-nearinfrared (UV-Vis-NIR) spectrometer (Agilent Cary 5000) was used to acquire optical absorption and transmission spectra. Optical absorption spectra were normalized by the π plasmon peak intensity for each sample. A MATLAB code^[57] was used to fit the SWCNT diameter distribution from the absorption spectra. The purity of s-SWCNTs was calculated with the same method which was described in the previous work.^[23] Besides, the collection area of 90% T film per hour was used to present the yield of SWCNTs, and the computing method for yield is shown in Supporting Information Text S1. A Nicolet Antaris IGS spectrometer (connected to the reactor outlet) was used to measure the Fourier transform infrared (FT-IR) spectra of the gas composition without SWCNTs. The resulting spectra represent the molecular absorption and transmission responses, creating the molecular fingerprint of the sample. A Raman spectrometer (Horiba Jobin-Yvon Labram HR 800), equipped with four excitation wavelengths, i.e., 488 nm, 514 nm, 633 nm, and 785 nm, was employed to acquire Raman spectra. In addition, Raman spectra were normalized by the Graphitic (G) band intensity and averaged from 3 random positions on each sample. The sparse s-SWCNTs were collected onto SiO_2 substrate by thermophoretic (TP) method^[43] for the length measurement with the scanning electron microscope (SEM, Zeiss Sigma VP) at an acceleration voltage of 1 kV. For further structural and morphological characterization, a JEM 2200FS (JEOL Ltd.) double Cs-corrected transmission electron microscope (TEM) was used for electron diffraction analysis operated at 80 kV and for high-resolution imaging operated at 200 kV. The chiral indices of an individual SWCNT can be extracted from its electron diffraction pattern based on an intrinsic-layer line spacing method developed earlier in the group.^[58]

Fabrication of Transistors: The back-gated transistors were fabricated by the commonly used photolithography and lift-off processes. The array of contacts was prefabricated on thermally oxidized silicon wafer with 100 nm of SiO_2 insulating layer and highly boron-doped back side of silicon wafer (Microchemicals GmbH) as the back gate. The source and drain electrodes were patterned by photolithography (Heidelberg MLA150) and 5 nm / 25 nm Ti/Pd were deposited by electron beam evaporation (Evaporator MASA IM-9912).^[38] Then, the dry and direct thermophoretic (TP) method was employed to deposit as-synthesized SWCNTs on the top of prefabricated arrays of electrodes.^[43] After SWCNTs deposition, the channel areas were defined by photolithography and the unwanted SWCNTs from outside channel area were etched away by an O_2/Ar plasma. Next, both FETs and TFTs chips were annealed at 200 °C for two h at ambient conditions to improve the contact between SWCNTs and electrodes. Finally, the electrical measurements were carried out at room temperature and ambient condition with a semi-automatic probe station (PA200, Karl Suss AG, Germany) which is equipped with a semiconductor parameter analyzer (Agilent 4168, USA).

Supporting Information

Supporting Information is available from the Wiley Online Library or from the author.

Acknowledgements

The research was supported by the Academy of Finland (316572, CNTstress), the Academy of Finland Flagship Programme (320167, PREIN), the Business Finland (ALDEL), the European Union's Horizon 2020 research and innovation program (965124, FEMTOCHIP) and GrapheneCore3 (881603). P.L. acknowledges the financial support from China Scholarship Council (No. 202006310007). The authors are grateful to Aalto University for their facilities and technical support at the OtaNano-NanoMicroscopy Center (Aalto-NMC) and the OtaNano-Micronova Nanofabrication Center. The authors sincerely thank Dr. Inoue Hirota, Dr. Karakasidis Anastasios, and Dr. Borghai Maryam for proof-reading.

Conflict of Interest

The authors declare no conflict of interest.

Data Availability Statement

The data that support the findings of this study are available in the supplementary material of this article.

Keywords

gas-phase synthesis, isopropanol, reproducibility, semiconducting single-walled carbon nanotubes, transistors

Received: March 23, 2023

Revised: April 12, 2023

Published online: May 26, 2023

- [1] R. F. Service, *Science* **2009**, *323*, 1000.
- [2] L. Liu, J. Han, L. Xu, J. Zhou, C. Zhao, S. Ding, H. Shi, M. Xiao, L. Ding, Z. Ma, C. Jin, Z. Zhang, L. M. Peng, *Science* **2020**, *368*, 850.
- [3] S. Datta, W. Chakraborty, M. Radosavljevic, *Science* **2022**, *378*, 733.
- [4] M. C. Lemme, D. Akinwande, C. Huyghebaert, C. Stampfer, *Nat. Commun.* **2022**, *13*, 1392.
- [5] C. Qiu, Z. Zhang, M. Xiao, Y. Yang, D. Zhong, L. M. Peng, *Science* **2017**, *355*, 271.
- [6] Y. Chen, M. Lyu, Z. Zhang, F. Yang, Y. Li, *ACS Cent. Sci.* **2022**, *8*, 1490.
- [7] Q. Cao, J. Tersoff, D. B. Farmer, Y. Zhu, S. J. Han, *Science* **2017**, *356*, 1369.
- [8] S. J. Tans, M. H. Devoret, H. Dai, A. Thess, R. E. Smalley, L. J. Geerligs, C. Dekker, *Nature* **1997**, *386*, 474.
- [9] G. Hills, C. Lau, A. Wright, S. Fuller, M. D. Bishop, T. Srimani, P. Kanhaiya, R. Ho, A. Amer, Y. Stein, D. Murphy, Arvind, A. Chandrakasan, M. M. Shulaker, *Nature* **2019**, *572*, 595.
- [10] A. D. Franklin, *Nature* **2013**, *498*, 443.
- [11] P. Avouris, Z. Chen, V. Perebeinos, *Nat. Nanotechnol.* **2007**, *2*, 605.
- [12] Y. Wang, D. Liu, H. Zhang, J. Wang, R. Du, T. T. Li, J. Qian, Y. Hu, S. Huang, *Nano Lett.* **2020**, *20*, 496.
- [13] Y. Wang, J. Wang, C. Ding, H. Zhang, R. Du, S. Zhang, J. Qian, Y. Hu, S. Huang, *Chem. Commun.* **2020**, *56*, 14259.
- [14] M. S. Arnold, A. A. Green, J. F. Hulvat, S. I. Stupp, M. C. Hersam, *Nat. Nanotechnol.* **2006**, *1*, 60.
- [15] T. G. S., F. A. D., A. A., *ACS Nano* **2013**, *7*, 2971.
- [16] M. Zheng, A. Jagota, M. S. Strano, A. P. Santos, P. Barone, S. G. Chou, B. A. Diner, M. S. Dresselhaus, R. S. McLean, G. B. Onoa, G. G.

- Samsonidze, E. D. Semke, M. Usrey, D. J. Watts, *Science* **2003**, *302*, 1545.
- [17] T. Lei, L. L. Shao, Y. Q. Zheng, G. Pitner, G. Fang, C. Zhu, S. Li, R. Beausoleil, H. S. P. Wong, T. C. Huang, K. T. Cheng, Z. Bao, *Nat. Commun.* **2019**, *10*, 2161.
- [18] D. M. Sun, M. Y. Timmermans, Y. Tian, A. G. Nasibulin, E. I. Kauppinen, S. Kishimoto, T. Mizutani, Y. Ohno, *Nat. Nanotechnol.* **2011**, *6*, 156.
- [19] L. Ding, A. Tselev, J. Wang, D. Yuan, H. Chu, T. P. McNicholas, Y. Li, J. Liu, *Nano Lett.* **2009**, *9*, 800.
- [20] Y. Che, C. Wang, J. Liu, B. Liu, X. Lin, J. Parker, C. Beasley, H.-S. S. P. Wong, C. Zhou, *ACS Nano* **2012**, *6*, 7454.
- [21] A. E. Islam, J. A. Rogers, M. A. Alam, *Adv. Mater.* **2015**, *27*, 7908.
- [22] F. Yang, M. Wang, D. Zhang, J. Yang, M. Zheng, Y. Li, *Chem. Rev.* **2020**, *120*, 2693.
- [23] E.-X. Ding, P. Liu, A. T. Khan, Q. Zhang, N. Wei, H. Jiang, E. I. Kauppinen, *Carbon* **2022**, *195*, 92.
- [24] W. Zhou, S. Zhan, L. Ding, J. Liu, *J. Am. Chem. Soc.* **2012**, *134*, 14019.
- [25] F. Yang, X. Wang, J. Si, X. Zhao, K. Qi, C. Jin, Z. Z. Zhang, M. Li, D. Zhang, J. Yang, Z. Z. Zhang, Z. Xu, L.-M. M. Peng, X. Bai, Y. Li, *ACS Nano* **2017**, *11*, 186.
- [26] B. Yu, C. Liu, P.-X. X. Hou, Y. Tian, S. Li, B. Liu, F. Li, E. I. Kauppinen, H.-M. M. Cheng, *J. Am. Chem. Soc.* **2011**, *133*, 5232.
- [27] W.-H. Chiang, R. M. Sankaran, *Nat. Mater.* **2009**, *8*, 882.
- [28] Y. Yao, X. Dai, R. Liu, J. Zhang, Z. Liu, *J. Phys. Chem. C* **2009**, *113*, 13051.
- [29] V. I. Artyukhov, E. S. Penev, B. I. Yakobson, *Nat. Commun.* **2014**, *5*, 4892.
- [30] Y. Liao, Z. Zhang, Q. Zhang, N. Wei, S. Ahmad, Y. Tian, E. I. Kauppinen, *ACS Appl. Nano Mater.* **2021**, *4*, 9673.
- [31] P.-X. Hou, W.-S. Li, S.-Y. Zhao, G.-X. Li, C. Shi, C. Liu, H.-M. Cheng, *ACS Nano* **2014**, *8*, 7156.
- [32] W. S. Li, P. X. Hou, C. Liu, D. M. Sun, J. Yuan, S. Y. Zhao, L. C. Yin, H. Cong, H. M. Cheng, *ACS Nano* **2013**, *7*, 6831.
- [33] X. Zhang, P. Li, H. Zhang, J. Liu, *Nano Res.* **2015**, *8*, 296.
- [34] F. Zhang, P.-X. Hou, C. Liu, B.-W. Wang, H. Jiang, M.-L. Chen, D.-M. Sun, J.-C. Li, H.-T. Cong, E. I. Kauppinen, H.-M. Cheng, *Nat. Commun.* **2016**, *7*, 11160.
- [35] S. D. Shandakov, A. V. Kosobutsky, M. S. Rybakov, O. G. Sevostyanov, D. M. Russakov, M. V. Lomakin, A. I. Vershina, I. M. Chirkova, *Carbon* **2018**, *126*, 522.
- [36] Z. Wang, Q. Zhao, L. Tong, J. Zhang, *J. Phys. Chem. C* **2017**, *121*, 27655.
- [37] A. D. Franklin, *Science* **2015**, *349*, aab2750.
- [38] N. Wei, P. Laiho, A. T. Khan, A. Hussain, A. Lyuleeva, S. Ahmed, Q. Zhang, Y. Liao, Y. Tian, E. X. Ding, Y. Ohno, E. I. Kauppinen, *Adv. Funct. Mater.* **2020**, *30*, 1907150.
- [39] Q. Cao, S. J. Han, G. S. Tulevski, A. D. Franklin, W. Haensch, *ACS Nano* **2012**, *6*, 6471.
- [40] T. Dürkop, S. A. Getty, E. Cobas, M. S. Fuhrer, *Nano Lett.* **2004**, *4*, 35.
- [41] X. Zhou, J.-Y. Park, S. Huang, J. Liu, P. L. McEuen, *Phys. Rev. Lett.* **2005**, *95*, 146805.
- [42] P. Stokes, S. I. Khondaker, *Appl. Phys. Lett.* **2010**, *96*, 083110.
- [43] P. Laiho, K. Mustonen, Y. Ohno, S. Maruyama, E. I. Kauppinen, *ACS Appl. Mater. Interfaces* **2017**, *9*, 20738.
- [44] A. Kaskela, K. Mustonen, P. Laiho, Y. Ohno, E. I. Kauppinen, *ACS Appl. Mater. Interfaces* **2015**, *7*, 28134.
- [45] S. Park, M. Vosguerichian, Z. Bao, *Nanoscale* **2013**, *5*, 1727.
- [46] L. S. Liyanage, H. Lee, N. Patil, S. Park, S. Mitra, Z. Bao, H. S. P. Wong, *ACS Nano* **2012**, *6*, 451.
- [47] X. Q. Li, S. Jiang, L. Zhang, M. K. Zou, Y. Jian, D. M. Sun, P. X. Hou, H. M. Cheng, C. Liu, *Chem. Eng. J.* **2022**, *450*, 137861.
- [48] H. Wang, P. Wei, Y. Li, J. Han, H. R. Lee, B. D. Naab, N. Liu, C. Wang, E. Adjianto, B. C. K. Tee, S. Morishita, Q. Li, Y. Gao, Y. Cui, Z. Bao, *Proc. Natl. Acad. Sci. U. S. A.* **2014**, *111*, 4776.
- [49] J. Zhang, C. Wang, C. Zhou, *ACS Nano* **2012**, *6*, 7412.
- [50] F. Molina-Lopez, T. Z. Gao, U. Kraft, C. Zhu, T. Öhlund, R. Pfattner, V. R. Feig, Y. Kim, S. Wang, Y. Yun, Z. Bao, *Nat. Commun.* **2019**, *10*, 2676.
- [51] X. Cao, C. Lau, Y. Liu, F. Wu, H. Gui, Q. Liu, Y. Ma, H. Wan, M. R. Amer, C. Zhou, *ACS Nano* **2016**, *10*, 9816.
- [52] Y. Choi, J. Kang, E. B. Secor, J. Sun, H. Kim, J. A. Lim, M. S. Kang, M. C. Hersam, J. H. Cho, *Adv. Funct. Mater.* **2018**, *28*, 1802610.
- [53] J. Tang, Q. Cao, G. Tulevski, K. A. Jenkins, L. Nela, D. B. Farmer, S. J. Han, *Nat. Electron.* **2018**, *1*, 191.
- [54] H. Wang, J. Mei, P. Liu, K. Schmidt, G. Jiménez-Osés, S. Osuna, L. Fang, C. J. Tassone, A. P. Zoombelt, A. N. Sokolov, K. N. Houk, M. F. Toney, Z. Bao, *ACS Nano* **2013**, *7*, 2659.
- [55] X. Wang, M. Wei, X. Li, S. Shao, Y. Ren, W. Xu, M. Li, W. Liu, X. Liu, J. Zhao, *ACS Appl. Mater. Interfaces* **2020**, *12*, 51797.
- [56] A. Kaskela, A. G. Nasibulin, M. Y. Timmermans, B. Aitchison, A. Papadimitratos, Y. Tian, Z. Zhu, H. Jiang, D. P. Brown, A. Zakhidov, E. I. Kauppinen, *Nano Lett.* **2010**, *10*, 4349.
- [57] Y. Tian, H. Jiang, J. v. Pfaler, Z. Zhu, A. G. Nasibulin, T. Nikitin, B. Aitchison, L. Khriachtchev, D. P. Brown, E. I. Kauppinen, *J. Phys. Chem. Lett.* **2010**, *1*, 1143.
- [58] H. Jiang, A. G. Nasibulin, D. P. Brown, E. I. Kauppinen, *Carbon* **2007**, *45*, 662.